Self-similar draining near a vertical edge

Nan Xue[1] and Howard A. Stone[1,*]

[1]*Department of Mechanical and Aerospace Engineering, Princeton University, Princeton, NJ 08544, USA*

(Dated: July 3, 2021)

When a liquid film drains on a vertical plate, the film becomes nonuniform near the vertical edge. Here we experimentally report the three-dimensional (3D) self-similar shape of this film. Based on the well-known 2D self-similar solution of a draining film far from the edge, we identify a new 3D self-similar scaling, which converts the PDE for the film thickness with three independent variables into an ODE. Interferometry is performed to measure the film thickness as a function of position and time, and the results are in excellent agreement with the theoretical predictions.

The gravitational drainage of a liquid film on a substrate is an example that has a two-dimensional (2D) self-similar solution for the film height as a function of position and time, as first recognized by Jeffreys [1]. In particular, by balancing gravitational forcing and viscous effects, the thickness of the draining film

$$h_J = (\mu x/\rho g t)^{1/2}, \tag{1}$$

where μ the fluid viscosity, x the vertical length of the film, ρ the fluid density and g the gravitational acceleration, which is known as *Jeffreys' solution* [1] (or the *Reynolds' thinning law* [2]). Certainly there are many examples of film drainage in other configurations, such as foams [3], tear films [4] and coating flows [5–7].

Self-similarity usually occurs where a system lacks a distinguished length scale or time scale [8]: e.g. unidirectional laminar flow near a planar wall (Stokes first problem) [9], corner flows [10], pinching of a liquid neck [11], liquid spreading by surface tension [12] or gravity [13, 14], etc. These self-similar solutions convert partial differential equations (PDEs) that describe the dynamics of the system with two independent variables to ordinary differential equations (ODEs) with only one independent variable. To the best of our knowledge, however, it is rare that a self-similar scaling converts a PDE with more than two independent variables into an ODE. One example of a similarity solution to a three-dimensional (3D) steady linear PDE is the case of rotary honing (the flow in a corner induced by the rotation in its plane) [15]. Our example below is for the case of an unsteady nonlinear PDE.

In this Letter, we report that when studying experimentally the draining film near the edges of a vertical substrate of finite width, the film profile shows self-similar features. For this edge configuration, there is no distinguished length scale in the vertical or horizontal direction. We identify a new self-similar scaling consistent with Jeffreys' solution in the far field: the PDE, which describes the film thickness profile with three independent variables, is converted to an ODE. This 3D self-similarity provides a universal law for the draining film shape with an edge throughout the drainage time, and is in excellent agreement with our experimental measurements.

In our experiments, to obtain a draining liquid film, fluid is injected onto a vertical glass slide. After injection, a portion of the fluid remains on the substrate as a liquid film and gradually drains under gravity. Fig. 1(a) shows a demonstration of the gravitationally draining film on a glass slide after injecting water with blue dye. Immediately after the injection, the liquid film is approximately horizontally uniform [$t = 0$ s, Fig. 1(a)]. The film then gradually drains and becomes nonuniform: for $t \geq 2$ s, the liquid film is darker near the edge of the substrate [Fig. 1(a, b)], which indicates that the film contains more dye and thus is thicker near the edge than in the middle. This suggests that the draining film shape varies horizontally near the edge, and is commonly observed as long as the draining film is confined at its edge [17]; see the schematic of the film shape in Fig. 2. The film shape near the edge looks similar to the liquid rims of a dry patch on an incline [18], but there is no inflow from outside and no dewetting of the liquid in our experiments.

While water might dewet on glass [17], silicone oil wets glass well and is used for further investigations in this Letter [see the material properties in the Supplemental Material (SM) [16]]. In the experiments, the draining silicone oil film is usually tens of micrometers in thickness, and interferometry is performed to measure the film thickness profile; see the sketch of the set-up in Fig. 1(c). A helium-neon laser (wavelength $\lambda = 633$ nm) illuminates the film, and the film thickness is measured according to the interferometric pattern formed by the reflected light rays from the air-oil and the glass-air interfaces. Characteristic interferometric patterns are displayed in Fig. 3(a-d). The film thickness difference between two neighboring fringes is $\lambda/(2n)$, where $n = 1.4$ is the refractive index of silicone oil, and this is used to reconstruct the film thickness profile; see details of the imaging in SM [16].

The interferometric images [Fig. 3(a)] imply a 3D shape of the draining film: far from the edge, the film has no memory of the initial film shape during the injection and quickly converges to Jeffrey's solution [17]; the film thickness varies near the edge, but the interferometric patterns are similar for different vertical positions x, times t or viscosities μ [Fig. 3(a-d)], which suggest similar film shapes. Extensive quantitative measurements are reported below. Inspired by these observations, we

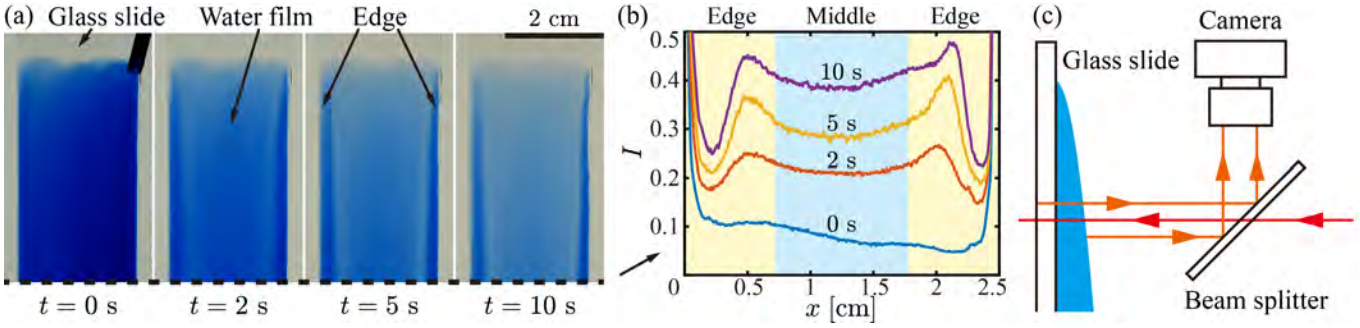

FIG. 1. Draining film on a vertical glass substrate. (a) A time series of water (with 0.5 wt% methylene blue hydrate) draining on a glass slide. A pipette moves horizontally along the glass substrate and gradually injected the fluid. The background light is provided by a LED panel. See the movie in SM [16]. (b) The horizontal variation of light intensity I (= grayscale/255) at different times t, along the bottom dashed line in (a). (c) A sketch of the interferometric set-up for measuring liquid film thickness.

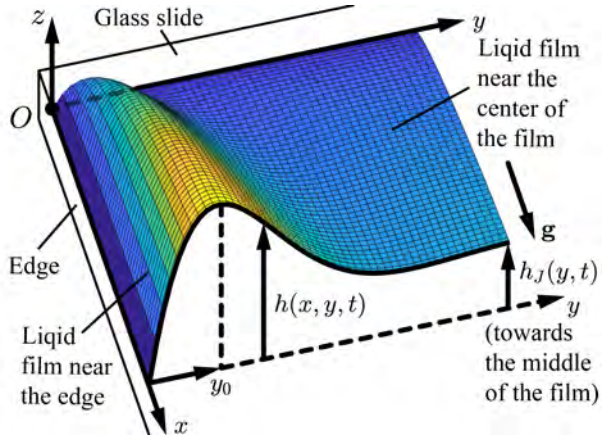

FIG. 2. A schematic of a vertical draining film near an edge.

construct a model to predict the draining film thickness accounting for the edge.

We consider a liquid film draining on a vertical substrate (Oxy); see the schematic in Fig. 2. Ox points downwards along the vertical edge of the plate. Oy points horizontally along the top pinned contact line of the liquid on the substrate. Assuming that $|\partial/\partial y| \gg |\partial/\partial x|$ near the edge, we start with a standard thin-film analysis where the film thickness $h(x, y, t)$ satisfies the nonlinear PDE [14]

$$3\mu\frac{\partial h}{\partial t} = -\gamma\frac{\partial}{\partial y}\left(h^3\frac{\partial^3 h}{\partial y^3}\right) - 3\rho g h^2\frac{\partial h}{\partial x}, \qquad (2)$$

where γ is the surface tension of the fluid. The three terms in Eq. (2) are viscous, surface tension and gravitational drainage terms, respectively. Note that Jeffreys' solution [Eq. (1)] is derived by balancing the viscous and gravitational drainage terms. As the surface tension term appears because of the edge configuration, we assume that the 3D film thickness profile $h(x, y, t)$ is self-similar and tied to Jeffreys' solution, according to

$$h(x, y, t) = h_J(x, t)F(\eta) = (\mu x/\rho g t)^{1/2}F(\eta), \qquad (3)$$

where $\eta = Ax^\alpha t^\beta y$ is a new scaled independent variable that combines the horizontal and vertical positions and time. Substituting Eq. (3) into Eq. (2), A, α and β are determined and the PDE in Eq. (2) with three independent variables becomes an ODE for $F(\eta)$,

$$-F + \frac{1}{4}\eta F' + \frac{2}{3}(F^3F''')' + F^3 - \frac{3}{4}\eta F^2F' = 0, \qquad (4)$$

where

$$\eta = \frac{(\rho g)^{3/8}t^{1/8}y}{\gamma^{1/4}\mu^{1/8}x^{3/8}}. \qquad (5)$$

The boundary conditions are $F = 0$ at $\eta = 0$ and $F = 1$ as $\eta \to \infty$ (this boundary condition in the far field represents two boundary conditions: at infinity, the diverging terms in the solution need to cancel each other, which yields two equations for the form of the solution; see details in SM [16]), i.e., the film thickness is zero at the edge and tends to $h_J(x, t)$ far from the edge.

Note that Eq. (4) is a fourth-order nonlinear ODE and has a possible singularity at the edge ($\eta = 0$) [8, 19]. Fully solving Eq. (4) requires examining the microscopic structure of the film near the edge [8], and a fourth boundary condition (e.g. the contact condition $\partial h/\partial y$ at the edge) is needed. Here we note that $F'(0)$ can be arbitrary since the contact line is at the edge. We set $F'(0) = 0$, which is consistent with a local solution to the ODE of the form $F(\eta) = C\eta^4$, where $C = 1/104$; see details in SM [16]. Rather than fully solving Eq. (4), our goal throughout this Letter is to demonstrate the macroscopic self-similar structure of the film away from the singularity. The microscopic structure does not affect the macroscopic film shape and the scaling [1, 12, 13]. The scaling [Eq. (5)], which converts the space as well as time, is our most important deduction. To demonstrate the structure of the solution of Eq. (4), we numerically compute the solution of Eq. (4) (details in SM [16]); see the gray solid line in Fig. 3(f).

Away from the edge, taking $f = F - 1$ where $|f| \ll 1$,

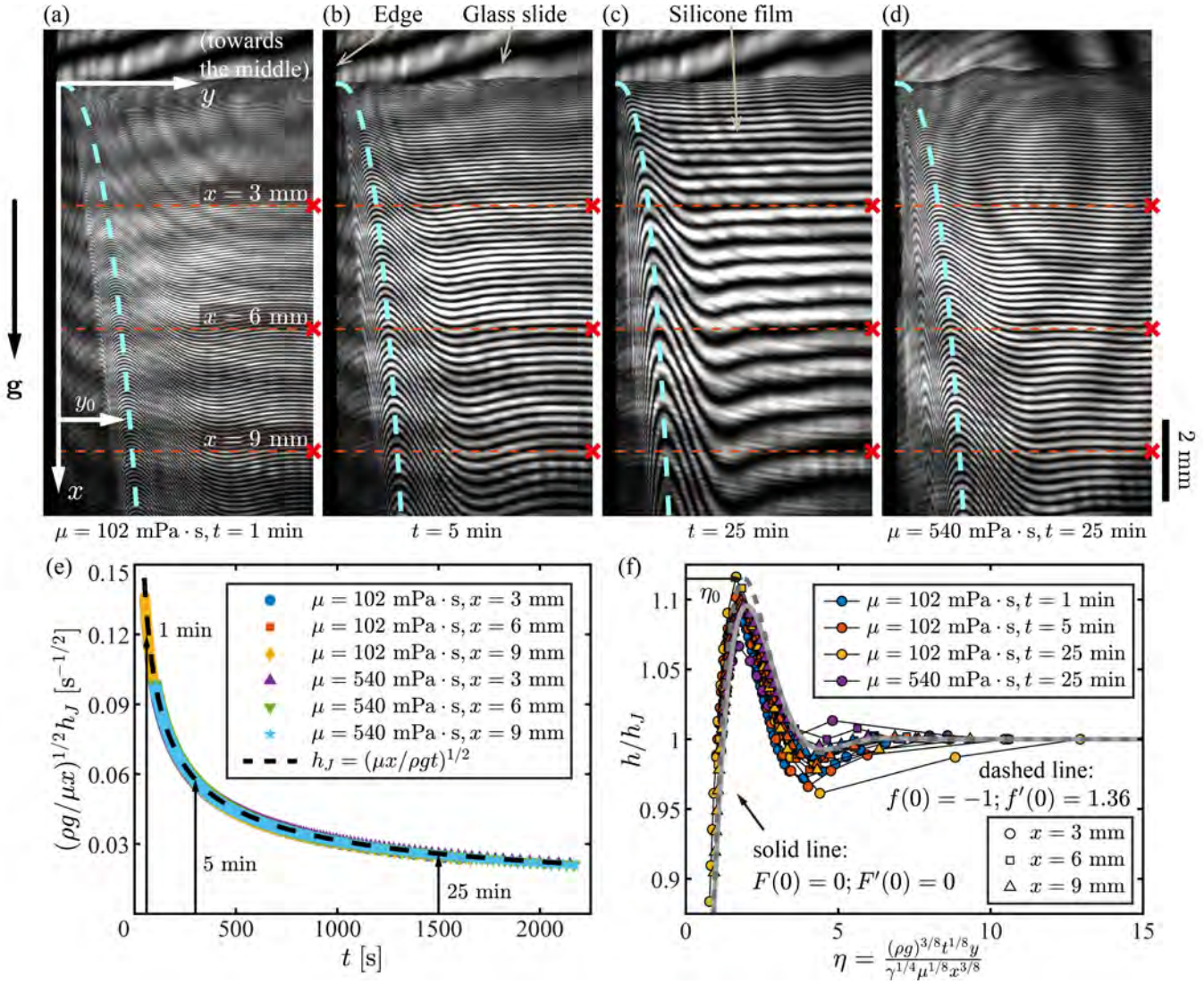

FIG. 3. Thickness profile of draining silicone oil films on glass substrates. (a-d) Interferometric images for silicone oil films with (a) $\mu = 102$ mPa · s and $t = 1$ min, (b) $\mu = 102$ mPa · s and $t = 5$ min, (c) $\mu = 102$ mPa · s and $t = 25$ min and (d) $\mu = 540$ mPa · s and $t = 25$ min, respectively. The blue dashed lines show the positions of the peaks of the draining films y_0. See the movies in SM [16]. (e) The normalized film thickness far from the edge, at $x = 3$, 6 and 9 mm and $y = 6.3$ mm [red crosses in (a-d)], as a function of time t. (f) The normalized film thickness h/h_J as a function of the normalized horizontal position η. The film thickness profiles on the red dashed lines in (a-d) are displayed. The gray solid and dashed lines show the solutions of Eq. (4) and Eq. (6), respectively (details in SM [16]).

Eq. (4) can be further linearized to obtain

$$f'''' - \frac{3}{4}\eta f' + 3f = 0, \tag{6}$$

which has analytical solutions in terms of hypergeometric functions [20] and demonstrates the first-order perturbation of the film thickness profile away from the edge; see details in SM [16].

Our scaling to the thin-film equation suggests a self-similar 3D shape of the draining film, which we have validated with the interferometric measurements of the film thickness. To reconstruct the film thickness profile, we first measure the film thickness near the middle of the substrate, far from the edge, at the fixed points $x = 3$, 6 and 9 mm and $y = 6.3$ mm [red crosses in Fig. 3(a-d)], respectively. During drainage, by counting the interferometric fringes that pass through a fixed point, the film thickness variation with time $\Delta h_J(x,t)$ is measured. In particular, we represent $\Delta h_J(x,t) = at^{-1/2} - b$, where a and b are fitting parameters, and the film thickness at the fixed point is then calculated as $h_J(x,t) = \Delta h_J(x,t) + b$. Such fitting provides robust estimations of the film thickness [17]. Fig. 3(e) shows the calculated normalized film thickness h_J as a function of time t, which is in excellent agreement with the prediction of Jeffreys' solution (dashed line).

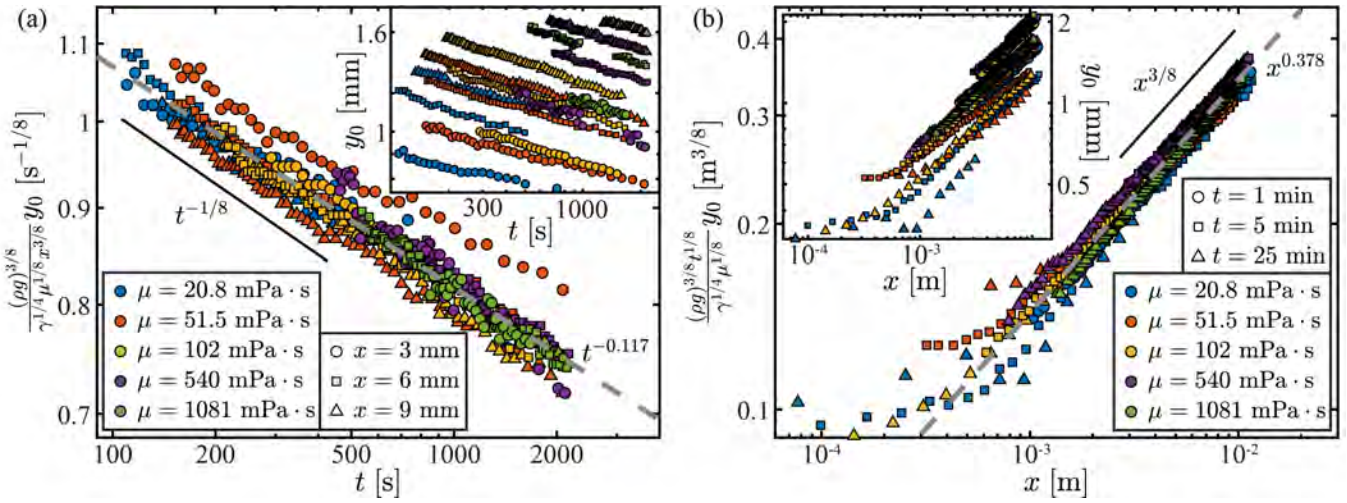

FIG. 4. The scaled horizontal position of the film peak as a function of (a) time t and (b) vertical position x (note the logarithmic axes). Five experiments with different silicone oils are performed (viscosity $\mu = 20.8$, 51.5, 102, 540 and 1081 mPa · s, respectively), and the scaled y_0, (a) $\frac{(\rho g)^{3/8}}{\gamma^{1/4}\mu^{1/8}x^{3/8}}y_0$ and (b) $\frac{(\rho g)^{3/8}t^{1/8}}{\gamma^{1/4}\mu^{1/8}}y_0$, are displayed respectively with (a) vertical positions $x = 3$, 6 and 9 mm and (b) times $t = 1$, 5 and 25 min. The insets show the unscaled y_0 with logarithmic axes.

Base on the calculated film thickness near the middle $h_J(x,t)$, the film thickness profile near the edge is then measured, by counting the fringes that are passed when horizontally moving from the middle to the edge, along the red dashed lines in Fig. 3(a-d). As a result, we find that the measured film shapes are self-similar: though the drainage times t, the vertical positions x and the viscosities μ vary in the different measurements, by normalizing the film thickness by Jeffreys' solution and normalizing the horizontal position by Eq. (5), the film shapes become approximately identical [Fig. 3(f)]. In general, from the edge ($\eta = 0$) to the middle ($\eta \to \infty$), the film thickness first increases until it reaches a peak [$\eta = \eta_0$; the positions of the peak are marked as blue dashed lines in Fig. 3(a-d)], and then decreases and oscillates towards $h_J(x,t)$. Near the edge, the horizontal variation of the film thickness is sharp and the fringes are narrow and beyond the resolution of the image analysis. Also, due to the sharp slope at the interface near the edge, the reflected light is not collected and dark regions are obtained [Fig. 3(a-d)]. We imaged the film shape with higher magnification, and the film thickness increased monotonically near the edge towards the peak (see SM [16]). The values of the film thickness displayed in Fig. 3(f) are close to the film thickness in the middle, i.e., $h/h_J \sim 1$. Therefore, the film thickness profile approximately satisfies the linearized Eq. (6), and we can construct a film thickness profile similar to the observed macroscopic film structure by Eq. (6). Both the computed numerical solution of Eq. (4) and the constructed analytical solution of the linearized Eq. (6) [the gray solid and dashed lines in Fig. 3(f)] reproduce well the details of our experimental measurements.

The film thickness profile presented in Fig. 3(f) shows that the film reaches a peak near the edge and then oscillates towards h_J away from the edge. The peaks of the film thickness act as a signature of the film shape near the edge; see the blue dashed lines in Fig. 3(a-d). Also, the self-similarity for the film thickness profile suggests that the normalized horizontal position η_0, where the film thickness is a maximum, should be identical for all draining films, regardless of t, x or μ. In the experiments, the horizontal positions of the peak y_0 are measured, with a large range of drainage times $t = 100$ to 2000 s, vertical positions $x = 0.1$ to 10 mm and fluid viscosities $\mu = 20$ to 1000 mPa · s. As $\eta_0 \approx 1.9$ [Fig. 3(f)], the expression of η [Eq. (5)] suggests that $y_0 \propto t^{-1/8}$ and $y_0 \propto x^{3/8}$, and these power-law behaviors are observed in the experiments: though the unscaled y_0 varies significantly with t or x (the insets in Fig. 4), we predict that the scaled variables collapse to master curves of power laws of t and x respectively (Fig. 4), according to Eq. (5). The experimental best fits for the scaled y_0 with t and x are, respectively, $y_0 \propto t^{-0.117\pm0.002}$ and $y_0 \propto x^{0.378\pm0.005}$ (dashed lines in Fig. 4). Note that the fitting of the scaled y_0 with x is processed for $x \geq 10^{-3}$ m, since the scaled y_0 deviates for $x < 10^{-3}$ m due to the uncertainties in the measurements and $|\partial/\partial y| \gg |\partial/\partial x|$ is not perfectly satisfied near the top contact line ($x = 0$). Both the best fits are close to our self-similar predictions and thus the universality of the 3D self-similar shape of the film near the edge is validated.

In this Letter, we determine the 3D self-similar shape for a gravitational draining liquid film near an edge on a vertical plate. While there is no distinguished length scale in the horizontal direction, based on Jeffreys' solution, a new self-similar scaling is derived, converting the unsteady nonlinear PDE that describes the film thickness profile with three independent variables into an ODE. The self-similar shape of the draining film is then val-

idated by interferometric experiments in a large range of t, x and μ. New power laws of time and vertical position are also established near the edge. According to Eq. (5), increasing the surface tension, viscosity and vertical length of the liquid film extends the region influenced by the edge, while increasing the density and drainage time shrinks this region. Further, the draining law applies to a draining water film that slowly dewets (see SM [16]). Also, inclining the plate with a small angle θ leads to identical results while the gravitational acceleration is modified as $g' = g\cos\theta$. This study provides guidelines for understanding and estimating draining films with edge configurations. The ideas presented may offer an approach to other thin film flows affected by edges.

We thank Niki Abbasi, Philippe Bourrianne, Min Pack and Lailai Zhu for valuable discussions. We thank the anonymous referees for their valuable suggestions and recommendations for improvement of the original manuscript. We thank the NSF for support from grant CBET-1804863.

* hastone@princeton.edu

[1] H. Jeffreys, "The draining of a vertical plate," Proc. Camb. Phil. Soc. **26**, 204–205 (1930).
[2] P. de Gennes, F. Brochard-Wyart, and D. Quéré, *Capillarity and Wetting Phenomena: Drops, Bubbles, Pearls, Waves* (Springer Science & Business Media, 2013).
[3] S. Cohen-Addad, R. Höhler, and O. Pitois, "Flow in foams and flowing foams," Annu. Rev. Fluid Mech. **45**, 241–267 (2013).
[4] R. J. Braun, "Dynamics of the tear film," Annu. Rev. Fluid Mech. **44**, 267–297 (2012).
[5] B. Levich and L. Landau, "Dragging of a liquid by a moving plate," Acta Physicochim. URS. **17**, 42 (1942).
[6] D. Quéré, "Fluid coating on a fiber," Annu. Rev. Fluid Mech. **31**, 347–384 (1999).
[7] S. J. Weinstein and K. J. Ruschak, "Coating flows," Annu. Rev. Fluid Mech. **36**, 29–53 (2004).
[8] J. Eggers and M. A. Fontelos, *Singularities: Formation, Structure, and Propagation*, Vol. 53 (Cambridge University Press, 2015).
[9] G. K. Batchelor, *An Introduction to Fluid Dynamics* (Cambridge University Press, 2000).
[10] H. K. Moffatt, "Viscous and resistive eddies near a sharp corner," J. Fluid Mech. **18**, 1–18 (1964).
[11] J. Eggers, "Universal pinching of 3D axisymmetric free-surface flow," Phys. Rev. Lett. **71**, 3458 (1993).
[12] L. H. Tanner, "The spreading of silicone oil drops on horizontal surfaces," J. Phys. D Appl. Phys. **12**, 1473 (1979).
[13] H. E. Huppert, "Flow and instability of a viscous current down a slope," Nature **300**, 427 (1982).
[14] B. R. Duffy and H. K. Moffatt, "A similarity solution for viscous source flow on a vertical plane," Eur. J. Appl. Math. **8**, 37–47 (1997).
[15] C. P. Hills and H. K. Moffatt, "Rotary honing: a variant of the Taylor paint-scraper problem," J. Fluid Mech. **418**, 119–135 (2000).
[16] See Supplemental Material [url] for movies, details and discussions for experiments, numerical computations and derivations, which includes Ref. [21].
[17] N. Xue, M. Y. Pack, and H. A. Stone, "Marangoni-driven film climbing on a draining pre-wetted film," J. Fluid Mech. **886**, A24 (2020).
[18] J. Sébilleau, L. Lebon, and L. Limat, "Stability of a dry patch in a viscous flowing film," Eur. Phys. J. Spec. Top. **166**, 139–142 (2009).
[19] A. A. Pahlavan, L. Cueto-Felgueroso, G. H. McKinley, and R. Juanes, "Thin films in partial wetting: internal selection of contact-line dynamics," Phys. Rev. Lett. **115**, 034502 (2015).
[20] H. A. Stone and C. Duprat, "Model problems coupling elastic boundaries and viscous flows," in *Fluid Structure Interactions in Low-Reynolds-Number Flows*, edited by C. Duprat and H. A. Stone (Royal Society of Chemistry, 2016) pp. 78–99.
[21] Y. Rotenberg, L. Boruvka, and A. W. Neumann, "Determination of surface tension and contact angle from the shapes of axisymmetric fluid interfaces," J. Colloid Interf. Sci. **93**, 169–183 (1983).